



Metasurface reflector enables room-temperature circularly polarized emission from VCSEL

XIANGLI JIA,¹ JONAS KAPRAUN,² JIAXING WANG,² JIPENG QI,² YIPENG JI,² AND CONNIE CHANG-HASNAIN^{2,*} 

¹Applied Science & Technology, University of California at Berkeley, Berkeley, California 94720, USA

²Berxel Photonics Co. Ltd., Shenzhen 518055, China

*connie.chang@berxel.com

Received 20 March 2023; revised 14 July 2023; accepted 19 July 2023; published 8 August 2023

While most lasers are linearly polarized, circularly polarized laser sources are crucial components for many optical applications such as biosensing, quantum technologies, and AR/VR. However, conventional methods for generating chiral light have limitations in device miniaturization. Vertical-cavity surface-emitting lasers (VCSELs), with their small footprint and surface emission feature, can be integrated with ultrathin metasurfaces for light manipulation, offering an opportunity to realize ultracompact chiral lasers. Here we report, to our knowledge, the first demonstration of chiral lasing from electrically pumped VCSELs at room temperature, without spin injection. This is enabled by incorporating a high-contrast chiral metasurface reflector as the VCSEL top mirror, favoring one specific circular polarization for lasing. Our demonstrated 940 nm VCSELs show stable single-mode chiral lasing and achieve a circular-polarization degree of up to 59%. This study provides a scalable approach for circular-polarization control of VCSELs and holds great promise for applications that desire ultracompact chiral emitters. © 2023 Optica Publishing Group under the terms of the [Optica Open Access Publishing Agreement](#)

<https://doi.org/10.1364/OPTICA.490176>

1. INTRODUCTION

Circularly polarized laser sources are essential building blocks for a wide range of applications in modern photonics, including biomedical sensing, quantum computing, data storage, and three-dimensional (3D) display [1–6]. However, generating chiral coherent light via conventional methods typically involves using linear polarizers and quarter-waveplates, which are both bulky and costly, and requires careful assembly for proper operation. This hinders the device miniaturization for portable and wearable applications. Therefore, there is a critical need for ultracompact chiral lasers with simple operation, to develop highly integrated and cost-effective optical systems.

To accomplish this goal, vertical-cavity surface-emitting lasers (VCSELs) offer a qualified design platform. VCSELs are among the most widely used semiconductor lasers, renowned for their outstanding features such as small footprint, low power consumption, ease of fabrication into arrays, and laterally isotropic geometry with circular symmetry. While the output polarization from a conventional VCSEL is not well-defined [7,8], several approaches for circular-polarization control have already been evaluated. Some approaches introduce polarization-dependent gain [9] by spin injection, either electrically or optically, to realize spin-lasers [10–15]. Other approaches utilize cavity designs with polarization-dependent reflectors based on 3D helical structures, such as cholesteric liquid crystals and sculptured thin films

[16–22]. However, all of these lasers suffer from complex structures that are not yet compatible with established optoelectronic technology.

In recent years, the emerging dielectric metasurfaces have attracted considerable attention [23–25], thanks to their ultrathin structure, low absorption loss, and extraordinary light manipulation capabilities, including polarization control. Moreover, these metasurfaces can be integrated on VCSELs [26–29], facilitated by the surface-normal emission geometry of the laser. This has brought new opportunities for ultracompact chiral laser design. One most straightforward approach is to use the integrated metasurface as a passive component to manipulate the output polarization, rather than altering the laser cavity [30]. Nevertheless, such design of passing through an external component drastically decreases the amount of usable light and thus reduces the overall power efficiency. Another approach is to modify the cavity design by incorporating chiral metasurfaces [31–34]. In this regard, chiral micro-lasers with a high degree of circular polarization have been demonstrated by electrically pumping chiral microcavities at cryogenic temperature [33], and optically pumping resonant metasurfaces doped with light-emitting molecules [34]. For practical applications, room-temperature chiral lasing under electrical pumping is preferred, yet it currently remains a missing piece in the literature.

Here we present, for the first time, to our knowledge, circularly polarized lasing from electrically pumped VCSELs at room temperature, without the need for spin injection. This is enabled by

incorporating a chiral high-contrast metasurface as a replacement for the VCSEL top reflector, which provides circular-polarization-dependent reflection. Leveraging established III-V fabrication processes, our demonstrated 940 nm VCSELs achieve a degree of circular polarization of up to 59%. These VCSELs show stable circular polarization and single transverse mode operation over a wide driving-current range. Therefore, this technique shows great promise for industrial and scientific applications that require ultracompact chiral lasers.

2. DESIGN

The working principle of our chiral VCSELs is based on circular-polarization-dependent reflection from the top mirror. According to basic laser physics, cavity mirror reflectivity can influence the threshold gain g_{th} of a VCSEL, which is given by

$$g_{th} = \frac{1}{\Gamma} \left[\alpha_i + \frac{1}{2L_{eff}} \ln \left(\frac{1}{R_1 R_2} \right) \right], \quad (1)$$

where Γ is the confinement factor, α_i is the internal loss, L_{eff} is the effective cavity length, and R_1 and R_2 are the power reflectivities of the top and bottom mirrors, respectively. Therefore, when the reflectivity of the top mirror differs for the two orthogonal circular polarizations, the threshold gain values for the two chiral modes will be different, resulting in circular-polarization-dependent lasing behavior. Specifically, if the reflectivity for right-handed circular polarization (RCP) is higher than that of left-handed circular polarization (LCP), the threshold gain for RCP will be relatively lower. As a result, the VCSEL will prefer to lase in RCP polarization, and vice versa.

Figure 1 shows a schematic of our GaAs-based chiral VCSEL, which shares a similar structure with our previous work on oxide spacer high-contrast grating (HCG) VCSELs [35]. The device comprises an active region sandwiched between a bottom mirror and a hybrid top mirror. The bottom mirror consists of 40 pairs of n -doped distributed Bragg reflector (DBR), while the hybrid top mirror is composed of a high-contrast chiral metasurface reflector and 9 pairs of p -doped DBR. The p -DBR facilitates current spreading [36] and offers a limited amount of reflectivity that is insensitive to circular polarization and not sufficient for lasing. The high-contrast chiral metasurface is the primary contributor to the overall reflectivity, and it also provides circular-polarization-sensitive reflection to the laser cavity. A ring-shaped p -contact on the top side and n -contact on the bottom side are used for

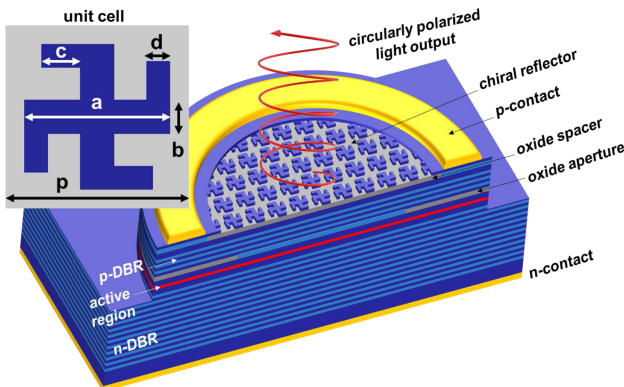


Fig. 1. Schematic of the proposed VCSEL featuring a chiral metasurface as the top reflector; the top-left inset shows a top view of the metasurface unit cell, with the geometric parameters labeled.

electrical injection. An oxide aperture is utilized to provide both current and optical confinement to the VCSEL. Details about the laser’s epitaxial structure and fabrication process can be found in Section 3.

The structure of the high-contrast chiral metasurface consists of gammadion-shaped GaAs nanostructures arranged in a square lattice, sitting on top of a low-index aluminum oxide spacer. Note that sufficient refractive-index contrast is essential for designing a high reflectivity mirror to support lasing [36]. The thickness of the GaAs layer is 220 nm, while the thickness of the oxide spacer is 150 nm. The inset of Fig. 1 depicts the top view of a unit cell of the chiral metasurface. The array of gammadion shapes, together with a substrate, exhibits structural chirality, meaning that it cannot be mapped to its mirror image via translation and rotation operations. The structure shows C_4 fourfold rotational symmetry but lacks any mirror symmetry. This ensures that the eigenpolarizations are circular states [37]. To design a circular-polarization-dependent reflector, we must achieve different optical reflection responses for RCP and LCP light incidence. According to theoretical studies based on reciprocity theorem, gammadion shapes with their C_4 symmetry will not result in reflectivity differences for zeroth-order reflections of RCP and LCP under normal incidence [38]. However, including higher-order diffraction allows for the successful demonstration of total reflection differences [39]. In the design of our chiral metasurface, the period p is chosen to be between the free space wavelength and the effective wavelength in the substrate. For normal incidence from the substrate side, light with different circular polarizations will experience different total reflectivities, mainly contributed by higher-order diffraction. Furthermore, we note that fabrication imperfections, which might cause structural symmetry breaking, also affect the reflectivity values. We performed 3D finite-difference-time-domain (FDTD) simulations using Ansys-Lumerical software, to obtain the total reflection behaviors of the chiral metasurface under RCP and LCP light incidence.

Circular-polarization-dependent reflection of the chiral metasurface can be controlled by geometrical parameters (a , b , c , d) for the gammadion shape and the period of the square lattice (p), as labeled in the inset of Fig. 1. Numerical simulations show that the geometric parameter c , which represents the length of the four orthogonally arranged arms of the gammadion shape, can be used to manipulate the sign of the reflectivity difference. As shown in Fig. 2, the reflectivity difference between RCP and LCP ($\Delta R = R_{RCP} - R_{LCP}$) is normalized by the average reflectivity for

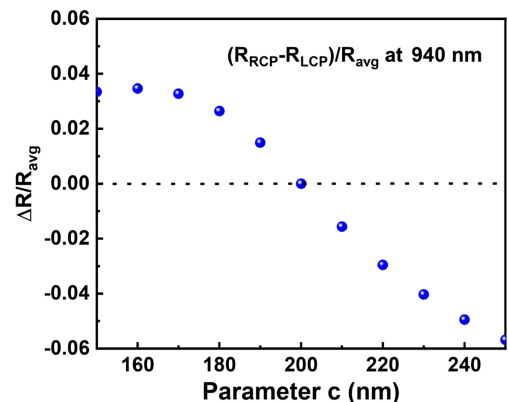


Fig. 2. Simulated reflectivity difference (normalized by average) between RCP and LCP polarization as a function of the parameter c .

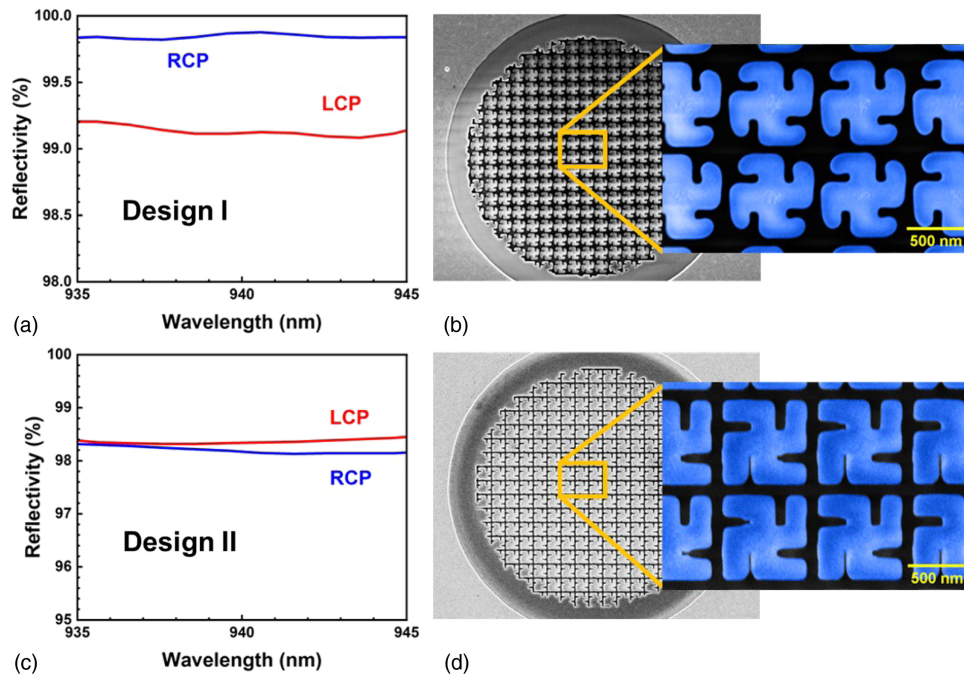


Fig. 3. (a) and (c) show the simulated RCP and LCP reflectivity spectra of a VCSEL top mirror with metasurface Design I and Design II. (b) and (d) are the top-view SEM images of the fabricated metasurfaces for Design I and Design II, respectively.

the two polarizations (R_{avg}) and plotted with respect to varying parameter c values. In these simulations, other parameters are fixed at the following values: $a = 690$ nm, $b = 200$ nm, $d = 140$ nm, and $p = 800$ nm. Additionally, the 15-nm-thick Al_2O_3 passivation protection layer on top of the metasurface is also included in the simulations. Reflectivity values at 940 nm are used, since our chiral VCSEL is designed for emission at 940 nm, which is a widely employed wavelength in the 3D sensing market. According to Fig. 2, when c is in the range of 150–200 nm, the reflectivity for RCP polarization is higher. When c falls within the range of 200–250 nm, the reflectivity for LCP polarization is higher. Therefore, the parameter c of the designed chiral metasurface has a significant effect on the preferred lasing polarization. The sensitivities of the reflectivity difference to the remaining parameters are relatively low, resulting in only minor variations in the polarization selectivity.

To demonstrate ultracompact chiral lasers, we investigated metasurface designs targeting VCSEL lasing in RCP or LCP polarization. Geometric parameters labeled in Fig. 1 were optimized to allow high reflectivity for the targeted circular polarization while keeping the reflectivity for the other polarization at relatively low values. To analyze the total reflection responses, it is necessary to design the chiral metasurface together with the nine pairs of top DBRs and the 15-nm-thick Al_2O_3 passivation protection layer. As shown in Figs. 3(a) and 3(c), the total reflectivity spectra with RCP and LCP light incident waves are simulated, for VCSEL top mirrors containing two different chiral metasurface designs: Design I ($a = 690$ nm, $b = 200$ nm, $c = 170$ nm, $d = 140$ nm, $p = 800$ nm) and Design II ($a = 690$ nm, $b = 180$ nm, $c = 250$ nm, $d = 150$ nm, $p = 820$ nm). We updated the lateral dimensions used in the simulations with values measured from fabricated devices, to include fabrication imperfections. We first note that the two designs meet the top mirror reflectivity requirement for a VCSEL to lase, which is typical above 99%.

We also calculated the reflectivity of a top mirror consisting only of nine pairs of DBRs, which is at most about 85%. For Design I in Fig. 3(a), the reflectivity to RCP is higher than the reflectivity to LCP around the targeted lasing wavelength, thus favoring lasing in RCP polarization. Similarly, Design II shows slightly higher reflectivity to LCP, favoring lasing in LCP polarization. This fascinating characteristic empowers the VCSEL mirror with circular-polarization selection function. Figures 3(b) and 3(d) show the top-view scanning electron microscope (SEM) image of the fabricated metasurfaces of our chiral VCSELs with Design I and Design II, respectively. The metasurface area size is $14 \mu\text{m}$ in diameter. The insets show close-up views of the metasurfaces.

3. FABRICATION

The epitaxial growth includes 40 pairs of Si:AlGaAs DBR, multiple InGaAs strained quantum wells used as an active region, a single 98% high Al oxide layer, nine pairs of C:AlGaAs DBR, a C:AlGaAs oxide spacer layer, and a C:metasurface epitaxial layer on a n^+ -GaAs substrate. The metasurface layer structure follows our previous work [35].

The fabrication process consists of several steps, including metasurface definition, oxide spacer formation, trench etch, oxide aperture formation, and metal contact depositions. First, the chiral metasurfaces are patterned on the top GaAs layer of the VCSEL epitaxial structure, by electron-beam lithography and chlorine-based inductively coupled plasma (ICP) etching down to the oxide spacer layer. A wet oxidation step follows, forming the low-refractive-index oxide spacer by selectively oxidizing the aluminum-rich layer underneath the metasurface. To prevent unintentional oxidation, a 10 nm layer of Al_2O_3 is deposited on top of the sample through atomic layer deposition (ALD).

Standard VCSEL processing is then employed to fabricate oxide-aperture-confined VCSELs. Trenches, with a depth of

2.5 μm , are defined by lithography and ICP etching, exposing another aluminum-rich layer. This layer then forms oxide apertures by selective wet oxidation, with aperture diameter of 7.5 μm . A 5 nm layer of aluminum oxide is deposited through ALD to serve as a passivation layer, bringing the cumulative thickness to 15 nm. The ALD aluminum oxide layer is then opened with buffered oxide etch, exposing a ring-shaped area that enables effective electrical access when forming contacts. Finally, Ti/Au metals are deposited on the top and bottom side of the chip using electron-beam evaporation, and a lift-off process is performed to pattern the p -type contacts.

4. MEASUREMENT RESULTS AND DISCUSSION

Chiral lasing from an electrically pumped VCSEL without spin injection has been demonstrated for the first time, to the best of our knowledge, at room temperature. We fabricated chiral VCSELs with metasurface reflectors utilizing Design I and Design II. To analyze the circular polarization of the emitted light, a quarter-waveplate and linear polarizer were inserted into the optical paths, following the measurement setup depicted in Fig. 5(b). The device characteristics for circular-polarization-resolved output power versus input current (L-I) curves are shown in Figs. 4(a) and 4(c). Design I emits predominantly RCP light, while Design II emits predominantly LCP light. From the L-I curves, the threshold currents are around 4.6 mA and 4.0 mA, respectively. For a device with Design II, thermal rollover occurs at current around 9 mA. Although the lasing threshold level of these devices is not particularly low compared to that of conventional VCSEL devices, possibly due to increased diffraction loss caused by the metasurface, it still suffices for low-power-consumption applications that require a chiral laser source.

While the handedness of the laser emissions matches well with our designs, we observed that the emitted light was not purely circularly polarized as initially expected. Instead, we detected elliptical polarization. We postulate that this deviation from pure circular polarization can be due to fabrication imperfections, which degrade the ideal C_4 symmetry to a lower structural symmetry. As a result, the eigenpolarization of the structure deviates from a purely circularly polarized state. The fabrication imperfections that can cause such symmetry degradation mainly refer to nonideal etched gammadion shapes with broken structural C_4 symmetry. In situations where circularly polarized light is incident on the metasurface reflectors with a symmetry lower than C_4 , the reflected light tends to be elliptically polarized. We confirmed this phenomenon by analyzing the reflection responses of the fabricated metasurface reflectors using lateral dimensions obtained from the SEM images. In comparing the simulated polarization orientation with the elliptical polarization observed in our VCSEL devices, we found consistency. Specifically, for the VCSEL with a metasurface reflector of Design I, where fabrication imperfections were present, showed a simulated polarization orientation of -54.2 deg, while the measured polarization orientation was -40.6 deg. Similarly, for Design II, the simulated and measured polarization orientations were 25.1 deg and 39.5 deg, respectively. These deviations are believed to be due to local etching depth variations, which were not included in our simulations. Despite this, the results demonstrate substantial consistency between theory and experiments. As for the minor symmetry degradation due to lateral misalignment between the metasurface and the cavity radial center, it shows a negligible impact on overall symmetry degradation, as detailed in the simulation results in Supplement 1. Apart from the fabrication imperfections impacting structural symmetry, the actual dimensions of the fabricated metasurfaces may deviate

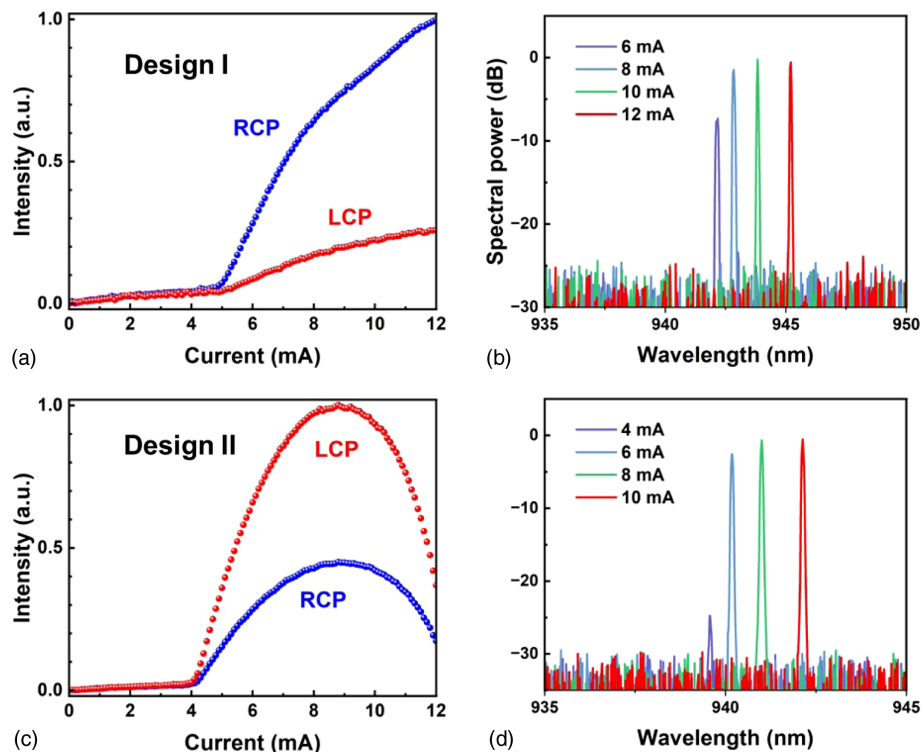


Fig. 4. Measurement results of chiral VCSEL devices with Design I (first row) and Design II (second row). (a) and (c) depict circular-polarization-resolved output light intensity as a function of the input current. (b), (d) are measured single-mode emission spectra under various bias currents.

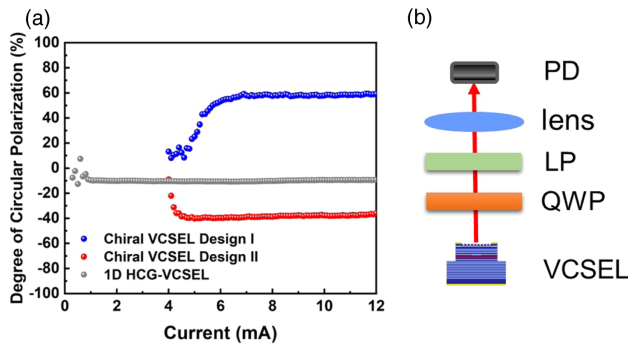


Fig. 5. (a) Degree of circular polarization (DOCP) as a function of the input current. (b) Schematic of the experimental setup with a linear polarizer (LP), quarter-waveplate (QWP), lens, and photodetector (PD).

from the designed values due to other kinds of imperfections, including aspect-ratio-dependent etching from the micro-loading effect and nonideal etched shapes such as rounded corners. These imperfections could affect the reflectivity values of the chiral reflectors, thereby affecting the chiral lasing performance. Besides, although the simulation results in Fig. 3 suggest that the metasurface reflector of Design I exhibits higher reflectivity than Design II, the experimental results in Fig. 4 reveal a lower threshold current for Design II compared to Design I. We note that these devices are fabricated on different chips, which resulted in nonidentical epilayer thickness and metasurface etching depth. However, in simulation, the thickness of the metasurface layer is fixed and perfect etching depth is assumed. Therefore, the simulated reflectivity values cannot be compared across devices on different chips for lasing threshold comparison, even though they are from the same epi-wafer.

Figures 4(b) and 4(d) show the laser emission spectra under different continuous-wave currents and reveal single transverse mode operation of the chiral VCSELs. The oxide aperture size is $7.5 \mu\text{m}$, and the side mode suppression ratio (SMSR) exceeded 25 dB. The single-mode feature is enabled by the oxide aperture and smaller modal reflectivities seen by higher-order transverse modes compared to the fundamental mode. The lasing wavelength red-shifts as the driving current increases, which is due to the current-induced thermal heating.

The degree of circular polarization can be calculated from $\text{DOCP} = (I_{\text{RCP}} - I_{\text{LCP}}) / (I_{\text{RCP}} + I_{\text{LCP}})$, where I_{RCP} and I_{LCP} are

the emission intensities in RCP and LCP polarization, respectively. Figure 5(a) shows the DOCP of laser emission for chiral VCSELs Design I and Design II as a function of the driving current. The DOCP of a control VCSEL with one-dimensional (1D) HCG is also shown for comparison. The HCG-VCSEL was fabricated using the same epi-wafer, and the HCG serves as the high reflection top mirror. The period of the HCG is 480 nm, and the grating bar width is 260 nm. Experimental results show that devices lacking a metasurface or HCG reflector failed to lase, indicating that a VCSEL top mirror with only nine pairs of DBR is insufficient for lasing. The HCG-VCSELs did not exhibit significant chiral lasing preferences, whereas the emission characteristics of the chiral-VCSELs were remarkably modified by the lithographically defined chiral metasurface reflectors. For chiral VCSELs operating just above the threshold current, the absolute value of DOCP gradually increases with the driving current and stabilizes under larger driving currents. The device with Design I emits in RCP polarization with a DOCP of up to 59%, and the device with Design II emits in LCP polarization with a DOCP of -40% (negative sign means LCP). The ability to maintain the DOCP at higher currents is a promising feature for applications that require higher optical powers. We also note that the DOCP value less than 100% is not indicative of theoretical constraints, but rather of practical challenges encountered during fabrication. Theoretically, it is indeed possible to achieve a high DOCP of 100% using our approach, provided the fabrication process is flawless and the C_4 symmetry of the structure is perfectly maintained.

In electrically pumped devices, the current needs to be transformed into carriers. It is important to recognize that the carrier reservoirs associated with right and left circularly polarized light are coupled through the spin-flip process. An excess of carriers in one reservoir results in spin flips to the opposite orientation at a certain rate, known as the spin-flip rate. Temperature-dependent DOCPs have previously been observed in experiments [40], which could be associated with the temperature dependence of the spin-flip rate. Physics and analysis of elliptically polarized states based on the spin-flip model [41] are beyond the scope of this paper and will be addressed in future work.

Table 1 compares our devices with previously demonstrated chiral lasers in the literature. Our technique offers several advantages, including electrical pumping, operation at room temperature, no

Table 1. Comparison with Other Demonstrated Chiral Lasers

Year	Pumping Method	Temp.	Spin Injection	Magnetic Field	DOCP	Key Fab. Step	Single Mode ^b	Refs.
1997	Optical	15 K	Optical	2 T	96%	—	Yes, L	[10]
1998	Optical	RT	Optical	No	50% ^a	—	Yes, L	[11]
2011	Optical	RT	Optical	No	96%	Unconventional GaAs (110) substrate	Yes	[12]
2016	Optical	RT	No	No	80%	E-beam litho.	Yes, L	[32]
2022	Optical	RT	No	No	98.9%	Slanted etching	Yes, L	[34]
2022	Electrical	1.8 K	No	No	90%	E-beam litho.	No	[33]
2022	Electrical	140 K/90 K	No	No	70%/28%	E-beam litho.	No	[40]
This work	Electrical	RT	No	No	59%	E-beam litho.	Yes, L & T	

^aDOCP reaches $\sim 80\%$ just above the threshold and rapidly decreases with increasing pumping power.

^bL, longitudinal mode; T, transverse mode.

reliance on spin injection or external magnetic fields, lithographically defined circular polarization, single transverse mode, and compatibility with current optoelectronic technology. A more detailed comparison is summarized in Table 1. There are still various possibilities for improving the design, such as higher DOCP, avoiding early thermal rollover, and reducing fabrication cost. To achieve even higher DOCP for our devices, one possible approach could involve adopting a simplified etching shape, such as a combination of rectangular pillars maintaining overall C_4 symmetry [32,33]. This could mitigate the fabrication challenges associated with the more complex gammadion shapes. Additionally, we could consider reducing the number of top DBR pairs, which are circular-polarization-insensitive, and further optimizing the chiral metasurfaces to increase the reflection difference between RCP and LCP light. Early thermal rollover can be treated with thermal engineering. Moreover, with a smallest feature size of 110 nm and a ± 20 nm tolerance, the fabrication process of the metasurfaces could be tailored to utilize deep-UV lithography for large-scale foundry manufacturing, making this technology more accessible for widespread applications.

5. CONCLUSION AND OUTLOOK

In this work, we introduced a novel approach for achieving chiral lasing by using circular-polarization-dependent reflectors. We utilized high-contrast chiral metasurfaces based on gammadion-shaped structures as VCSEL top mirrors, enabling circular-polarization control. We showed that the dominating circular polarization of the emitted light could be controlled by mainly adjusting a single geometric parameter of the gammadion shapes. We successfully applied this methodology to design chiral VCSELs for 940 nm emission and presented simulation and experimental results. Our fabricated devices enabled, to our knowledge, the first demonstration of chiral lasing from electrically pumped VCSELs at room temperature, without spin injection or magnetic fields. The devices exhibit single transverse mode operation and achieve a maximum degree of circular polarization of 59%. With the advantage of simple operation and small footprint, our chiral VCSELs mark a significant step towards ultracompact chiral laser sources for portable and wearable applications.

Furthermore, this approach is wavelength scalable and can be applied across a wide range of wavelengths. For future work, it is also feasible to design chirality switchable VCSELs, by utilizing a combination of wavelength-dependent polarization selectivity and thermal shift of the lasing wavelength. This creates new opportunities for chiral lasers in data communication applications. In conclusion, we believe that our proposed VCSELs with lithography-defined circular-polarization emission will be a valuable tool in the field of photonics and open up new avenues for research and development.

Acknowledgment. We thank the Berkeley Marvell Nanofabrication Laboratory for fabrication support.

Disclosures. The authors declare no conflicts of interest.

Data availability. Data underlying the results presented in this paper are not publicly available at this time but may be obtained from the authors upon reasonable request.

Supplemental document. See Supplement 1 for supporting content.

REFERENCES

- X. Zhan, F.-F. Xu, Z. Zhou, Y. Yan, J. Yao, and Y. S. Zhao, "3D laser displays based on circularly polarized lasing from cholesteric liquid crystal arrays," *Adv. Mater.* **33**, 2104418 (2021).
- C. D. Stanciu, F. Hansteen, A. V. Kimel, A. Kirilyuk, A. Tsukamoto, A. Itoh, and T. Rasing, "All-optical magnetic recording with circularly polarized light," *Phys. Rev. Lett.* **99**, 047601 (2007).
- B. Kunnen, C. Macdonald, A. Doronin, S. Jacques, M. Eccles, and I. Meglinski, "Application of circularly polarized light for non-invasive diagnosis of cancerous tissues and turbid tissue-like scattering media," *J. Biophoton.* **8**, 317–323 (2015).
- D. Bouwmeester, J.-W. Pan, K. Mattle, M. Eibl, H. Weinfurter, and A. Zeilinger, "Experimental quantum teleportation," *Nature* **390**, 575–579 (1997).
- C. He, H. He, J. Chang, B. Chen, H. Ma, and M. J. Booth, "Polarisation optics for biomedical and clinical applications: a review," *Light Sci. Appl.* **10**, 194 (2021).
- J. F. Sherson, H. Krauter, R. K. Olsson, B. Julsgaard, K. Hammerer, I. Cirac, and E. S. Polzik, "Quantum teleportation between light and matter," *Nature* **443**, 557–560 (2006).
- C. Chang-Hasnain, J. Harbison, L. Florez, and N. Stoffel, "Polarisation characteristics of quantum well vertical cavity surface emitting lasers," *Electron. Lett.* **27**, 163–165 (1991).
- M. Shimizu, F. Koyama, and K. Iga, "Polarization characteristics of MOCVD grown GaAs/GaAlxS CBH surface emitting lasers," in *Integrated and Guided Wave Optics* (Optica, 1988), paper WA3.
- J. M. Ostermann and R. Michalzik, "Polarization control of vcsels," in *VCSELs: Fundamentals, Technology and Applications of Vertical-Cavity Surface-Emitting Lasers* (Springer, 2013), pp. 147–179.
- S. Hallstein, J. Berger, M. Hilpert, H. Schneider, W. Rühle, F. Jahnke, S. Koch, H. Gibbs, G. Khitrova, and M. Oestreich, "Manifestation of coherent spin precession in stimulated semiconductor emission dynamics," *Phys. Rev. B* **56**, R7076–R7079 (1997).
- H. Ando, T. Sogawa, and H. Gotoh, "Photon-spin controlled lasing oscillation in surface-emitting lasers," *Appl. Phys. Lett.* **73**, 566–568 (1998).
- S. Iba, S. Koh, K. Ikeda, and H. Kawaguchi, "Room temperature circularly polarized lasing in an optically spin injected vertical-cavity surface-emitting laser with (110) GaAs quantum wells," *Appl. Phys. Lett.* **98**, 081113 (2011).
- N. C. Gerhardt and M. R. Hofmann, "Spin-controlled vertical-cavity surface-emitting lasers," *Adv. Opt. Technol.* **2012**, 268949 (2012).
- I. Žutić, G. Xu, M. Lindemann, P. E. F. Junior, J. Lee, V. Labinac, K. Stojić, G. M. Sipahi, M. R. Hofmann, and N. C. Gerhardt, "Spin-lasers: spintronics beyond magnetoresistance," *Solid State Commun.* **316–317**, 113949 (2020).
- M. Holub and P. Bhattacharya, "Spin-polarized light-emitting diodes and lasers," *J. Phys. D* **40**, R179–R203 (2007).
- I. J. Hodgkinson, M. Arnold, M. W. McCall, and A. Lakhtakia, "Chiral mirror and optical resonator designs for circularly polarized light: suppression of cross-polarized reflectances and transmittances," *Opt. Commun.* **210**, 201–211 (2002).
- Y. Tanaka, H. Takano, and T. Kurokawa, "Circular polarization resonator based on cholesteric liquid crystal," *Jpn. J. Appl. Phys.* **43**, 1062–1067 (2004).
- Y. Zhou, Y. Huang, and S.-T. Wu, "Enhancing cholesteric liquid crystal laser performance using a cholesteric reflector," *Opt. Express* **14**, 3906–3916 (2006).
- V. I. Kopp, Z.-Q. Zhang, and A. Z. Genack, "Lasing in chiral photonic structures," *Prog. Quantum Electron.* **27**, 369–416 (2003).
- V. I. Kopp, B. Fan, H. Vithana, and A. Z. Genack, "Low-threshold lasing at the edge of a photonic stop band in cholesteric liquid crystals," *Opt. Lett.* **23**, 1707–1709 (1998).
- C.-T. Wang and T.-H. Lin, "Polarization-tunable chiral nematic liquid crystal lasing," *J. Appl. Phys.* **107**, 123102 (2010).
- Y. Zhu, F. Zhang, J. Liu, J. D. Zhang, A. Lakhtakia, and J. Xu, "Stable circularly polarized emission from a vertical-cavity surface-emitting laser with a chiral reflector," *Appl. Phys. Express* **5**, 032102 (2012).
- D. Lin, P. Fan, E. Hasman, and M. L. Brongersma, "Dielectric gradient metasurface optical elements," *Science* **345**, 298–302 (2014).
- A. Arbabi, E. Arbabi, Y. Horie, S. M. Kamali, and A. Faraon, "Planar metasurface retroreflector," *Nat. Photonics* **11**, 415–420 (2017).

25. P. Genevet, F. Capasso, F. Aieta, M. Khorasaninejad, and R. Devlin, "Recent advances in planar optics: from plasmonic to dielectric metasurfaces," *Optica* **4**, 139–152 (2017).
26. Y.-Y. Xie, P.-N. Ni, Q.-H. Wang, Q. Kan, G. Briere, P.-P. Chen, Z.-Z. Zhao, A. Delga, H.-R. Ren, H.-D. Chen, and C. Xu, "Metasurface-integrated vertical cavity surface-emitting lasers for programmable directional lasing emissions," *Nat. Nanotechnol.* **15**, 125–130 (2020).
27. D. Wen and K. B. Crozier, "Metasurfaces 2.0: laser-integrated and with vector field control," *APL Photon.* **6**, 080902 (2021).
28. K. Li, Y. Rao, C. Chase, W. Yang, and C. J. Chang-Hasnain, "Monolithic high-contrast metastructure for beam-shaping VCSELs," *Optica* **5**, 10–13 (2018).
29. M. S. Seghilani, M. Myara, M. Sellahi, L. Legratiet, I. Sagnes, G. Beaudoin, P. Lalanne, and A. Garnache, "Vortex laser based on III-V semiconductor metasurface: direct generation of coherent Laguerre-Gauss modes carrying controlled orbital angular momentum," *Sci. Rep.* **6**, 38156 (2016).
30. D. Wen, J. Meng, J. J. Cadusch, and K. B. Crozier, "VCSELs with on-facet metasurfaces for polarization state generation and detection," *Adv. Opt. Mater.* **9**, 2001780 (2021).
31. A. Maksimov, I. Tartakovskii, E. Filatov, S. Lobanov, N. Gippius, S. Tikhodeev, C. Schneider, M. Kamp, S. Maier, S. Höfiling, and V. D. Kulakovskii, "Circularly polarized light emission from chiral spatially-structured planar semiconductor microcavities," *Phys. Rev. B* **89**, 045316 (2014).
32. A. Demenev, V. Kulakovskii, C. Schneider, S. Brodbeck, M. Kamp, S. Höfiling, S. Lobanov, T. Weiss, N. Gippius, and S. Tikhodeev, "Circularly polarized lasing in chiral modulated semiconductor microcavity with GaAs quantum wells," *Appl. Phys. Lett.* **109**, 171106 (2016).
33. A. Maksimov, E. Filatov, I. I. Tartakovskii, V. Kulakovskii, S. Tikhodeev, C. Schneider, and S. Höfiling, "Circularly polarized laser emission from an electrically pumped chiral microcavity," *Phys. Rev. Appl.* **17**, L021001 (2022).
34. X. Zhang, Y. Liu, J. Han, Y. Kivshar, and Q. Song, "Chiral emission from resonant metasurfaces," *Science* **377**, 1215–1218 (2022).
35. K. T. Cook, J. Qi, J. Wang, N. Cabello, and C. J. Chang-Hasnain, "Novel oxide spacer high-contrast grating VCSELs," in *CLEO: Science and Innovations* (Optical Society of America, 2018), paper STu3Q.6.
36. M. C. Huang, Y. Zhou, and C. J. Chang-Hasnain, "A surface-emitting laser incorporating a high-index-contrast subwavelength grating," *Nat. Photonics* **1**, 119–122 (2007).
37. C. Menzel, C. Rockstuhl, and F. Lederer, "Advanced jones calculus for the classification of periodic metamaterials," *Phys. Rev. A* **82**, 053811 (2010).
38. B. Bai, Y. Svirko, J. Turunen, and T. Vallius, "Optical activity in planar chiral metamaterials: theoretical study," *Phys. Rev. A* **76**, 023811 (2007).
39. A. Y. Zhu, W. T. Chen, A. Zaidi, Y.-W. Huang, M. Khorasaninejad, V. Sanjeev, C.-W. Qiu, and F. Capasso, "Giant intrinsic chiro-optical activity in planar dielectric nanostructures," *Light Sci. Appl.* **7**, 17158 (2018).
40. A. A. Maksimov, E. V. Filatov, and I. I. Tartakovskii, "Temperature dependence of circularly polarized radiation of an injection semiconductor laser," *JETP Lett.* **116**, 500–504 (2022).
41. M. San Miguel, Q. Feng, and J. V. Moloney, "Light-polarization dynamics in surface-emitting semiconductor lasers," *Phys. Rev. A* **52**, 1728–1739 (1995).